

# SMR: Satisfied Machine Ratio Modeling for Machine Recognition-Oriented Image and Video Compression

Qi Zhang<sup>1</sup>, Shanshe Wang<sup>1</sup>, Xinfeng Zhang<sup>2</sup>, Chuanmin Jia<sup>3</sup>, Jingshan Pan<sup>4</sup>, Siwei Ma<sup>1,5</sup>, and Wen Gao<sup>1,5</sup>

<sup>1</sup> National Engineering Research Center of Visual Technology, Peking University, Beijing, China

<sup>2</sup> University of Chinese Academy of Sciences, Beijing, China

<sup>3</sup> Wangxuan Institute of Computer Technology, Peking University, Beijing, China

<sup>4</sup> National Supercomputer Center in Jinan, Jinan, China

<sup>5</sup> Peng Cheng Laboratory, Shenzhen, China

qizhang@stu.pku.edu.cn, xfzhang@ucas.ac.cn, panjsh@sdas.org,  
{sswang, cmjia, swma, wgao}@pku.edu.cn

## Abstract

*Tons of images and videos are fed into machines for visual recognition all the time. Like human vision system (HVS), machine vision system (MVS) is sensitive to image quality, as quality degradation leads to information loss and recognition failure. In recent years, MVS-targeted image processing, particularly image and video compression, has emerged. However, existing methods only target an individual machine rather than the general machine community, thus cannot satisfy every type of machine. Moreover, the MVS characteristics are not well leveraged, which limits compression efficiency. In this paper, we introduce a new concept, Satisfied Machine Ratio (SMR), to address these issues. SMR statistically measures the image quality from the machine's perspective by collecting and combining satisfaction scores from a large quantity and variety of machine subjects, where such scores are obtained with MVS characteristics considered properly. We create the first large-scale SMR dataset that contains over 22 million annotated images for SMR studies. Furthermore, a deep learning-based model is proposed to predict the SMR for any given compressed image or video frame. Extensive experiments show that using the SMR model can significantly improve the performance of machine recognition-oriented image and video compression. And the SMR model generalizes well to unseen machines, compression frameworks, and datasets.*

## 1. Introduction

Intelligent machines are exploding in recent years. Many of these machines are designed to understand images and

videos. They can recognize image content by extracting knowledge from pixels, and their recognitions are used to solve many real-world problems like facial payment and cancer detection. With the development of modern machine vision techniques, machines have already surpassed humans in recognition capability [15], and are becoming even more and more powerful.

Humans seek high quality images and videos to satisfy their insatiable visual appetite. Similarly, machines pursue high quality input visual data for successful recognitions. However, in the real world, due to the limitations on transmission and storage, images and videos are typically compressed before being fed into machines, which brings distortions to visual signals and degrades the quality. Although a machine can be trained to fit for distorted data, its generalizability will be poor [13]. Therefore, improving the compression performance is necessary, and several compression standards are established, including JPEG [43], AVC [45], HEVC [36], VVC [3], AV1 [14], and AVS3 [49].

Unfortunately, none of the commonly-used mature standards are specifically optimized for machines. In recent years, several MVS-oriented compression methods have been proposed to fill this gap [47], which can be divided into two categories. The first is to modify current compression frameworks, such as refining parameter selection [23, 26], rate-distortion optimization [10, 50, 52], and bit allocation [4, 11, 19] modules. The second is to learn an end-to-end compression network with a machine vision task-specific constraint [1, 9, 30, 42]. Based on these explorations, the standardization of visual signal compression for machines has also begun, namely Video Coding for Machines (VCM) [12]. However, these methods usually have two drawbacks. First, they are developed and evaluated with only one or a

few machines involved, thus lacking the generality. Second, the MVS characteristics are not well exploited and utilized, thus limiting the performance.

Reviewing traditional compression schemes, perceptual compression for humans is a good example that overcomes these drawbacks. More specifically, HVS has some inherent flaws that cannot notice small differences between clean and distorted images. To capitalize on this attribute, a concept known as Just Noticeable Difference (JND) was introduced and modeled [20, 27]. JND gives the maximum distortion that HVS cannot perceive, thereby establishing a theoretically perfect operation point for compression. As different human subjects have distinctive visual acuities, JND is further extended to Satisfied User Ratio (SUR) [8, 44, 53]. SUR is calculated from the cumulative distribution of JND locations obtained from a large population of human subjects, thus measures subjective image quality more generally and correctly. Moreover, compared with a single JND point, SUR forms a continuous and deterministic model that provides multiple operation points for compression, making it more applicable. More recently, a few works demonstrate the existence of JND for machines [21, 51] and reveal its potential for MVS-oriented visual signal compression. Yet, the SUR for machines has not been explored.

In this work, we make the first attempt. A new concept, Satisfied Machine Ratio (SMR), is introduced to model the general MVS behavior. We treat different machines as different subjects and combine their satisfaction scores to get a final SMR score. Each satisfaction score demonstrates the MVS characteristics of the corresponding machine. As a result, SMR measures image and video quality from the machine’s perspective accurately. We create a large-scale dataset for SMR studies and propose a deep learning-based model to predict the SMR for any given compressed image or video frame. The predicted SMR can be used reversely to guide the compression and improve the performance. The dataset and models will be released to the public. Our contributions can be summarized as follows.

- To the best of our knowledge, we are the first to introduce the concept of SMR and give its mathematical formulation, which successfully models the MVS behaviors of the general machine community.
- We build a large-scale SMR dataset that contains over 22 million images with SMR annotations obtained from 58 to 72 different machine subjects, which facilitates future SMR studies.
- We propose a deep learning-based SMR prediction model. Using the estimated SMR to reversely guide compression, we can achieve a basic BD-rate saving of 25.7% and BD-SMR gain of 0.038. Extensive experiments demonstrate the proposed SMR model’s generalizability to different data domains.

## 2. Satisfied Machine Ratio

We begin with defining SMR. Let  $I_0$  be the pristine image or video frame that is compressed into several distorted variants  $I_{q_1}, I_{q_2}, \dots, I_{q_n}$ , where  $q_i$  denotes a certain quality level that deteriorates as  $i$  increases. Any machine  $M_j$  in the infinite set  $\mathbb{M}$  containing all machines has a satisfaction score to  $I_{q_i}$ , which can be denoted as

$$S(M_j; I_{q_i}), \quad (1)$$

where  $S(\cdot)$  is a function for computing the satisfaction score. Then, the SMR of  $I_{q_i}$  can be calculated as

$$SMR(I_{q_i}) = \frac{|\{M_j \mid S(M_j; I_{q_i}) \geq T_S\}|}{|\mathbb{M}|}, \quad (2)$$

where  $T_S$  is a threshold value for satisfaction score, and  $|\cdot|$  counts the elements in the set. As such, SMR statistically presents the proportion of machines that are satisfied with a certain level of image quality.

In this paper, we make an initial attempt to investigate SMR for image classification, a fundamental machine recognition task. The satisfaction score function for this specific task is determined as

$$S(M_j; I_{q_i}) = \begin{cases} 1, & \text{if Top-1}(M_j(I_{q_i})) \subseteq \text{Top-K}(M_j(I_0)), \\ 0, & \text{otherwise} \end{cases}, \quad (3)$$

where  $M_j(I_{q_i})$  is the output probabilities for each class from  $M_j$  given  $I_{q_i}$  as input, and  $\text{Top-1}(\cdot)$  and  $\text{Top-K}(\cdot)$  return the set of class indices with top-1 and top- $K$  probability values, respectively.  $T_S$  is set to 0 when computing the final SMR with Eq. (2).

It should be noticed that the ground truth class labels annotated by humans are not used in SMR calculations for three reasons. First, humans may make mistakes when annotating ground truth labels, which can result in inaccurate and unreliable SMR modeling. Second, the prediction difference on pristine images and their distorted variants naturally reveals the MVS characteristics for a specific machine such as the capability and robustness. Third, without the need for annotations, we can study the SMR profiles with more much visual data, even unsupervisedly.

Eq. (3) can locate the JND point of  $I_0$  for  $M_j$  implicitly. More specifically, as  $i$  increases,  $S(M_j; I_{q_i})$  is more likely to be 0. Once the first 0 is calculated, the corresponding  $q_i$  should point to the JND. However, it is interesting to find that for a large number of images, even  $S(M_j; I_{q_i})$  has already returned 0,  $S(M_j; I_{q_k})$  can still equal to 1, where  $k > i$ . Therefore, many images do not have a machine **just** noticeable difference point. But in any case, Eq. (3) can reflect the MVS characteristics.

Version	Category	Name
v1	Classical CNN	AlexNet [22]
		VGG-11, VGG-13, VGG-16, VGG-19, VGG-11-bn, VGG-13-bn, VGG-16-bn, VGG-19-bn [35]
		GoogLeNet [37]; Inception-v3 [38]
		ResNet-18, ResNet-34, ResNet-50, ResNet-101, ResNet-152 [16]
		ResNeXt-50-32x4d, ResNeXt-101-32x8d [46]; Wide-ResNet-50, Wide-ResNet-101 [48]
	DenseNet-121, DenseNet-161, DenseNet-169, DenseNet-201 [18]	
	Lightweight Network	ShuffleNet-v2-x0.5, ShuffleNet-v2-x1.0 [31]
		MobileNet-v2 [34], MobileNet-v3-small, MobileNet-v3-large [17]
	Network Architecture Search	MNASNet-0.5, MNASNet-1.0 [39]
		EfficientNet-b0, EfficientNet-b1, EfficientNet-b3, EfficientNet-b5, EfficientNet-b7 [40]
		RegNet-x-400mf, RegNet-x-800mf, RegNet-x-1.6gf, RegNet-x-3.2gf, RegNet-x-8gf, RegNet-x-16gf, RegNet-x-32gf; RegNet-y-400mf, RegNet-y-800mf, RegNet-y-1.6gf, RegNet-y-3.2gf, RegNet-y-8gf, RegNet-y-16gf, RegNet-y-32gf [33]
	Transformer	ViT-b-16, ViT-b-32, ViT-l-16, ViT-l-32 [6]
Modern CNN	ConvNeXt-tiny, ConvNeXt-small, ConvNeXt-base, ConvNeXt-large [29]	
v2	Classical CNN	ResNeXt-101-64x4d
	Lightweight Network	ShuffleNet-v2-x1.5, ShuffleNet-v2-x2.0
	Network Architecture Search	MNASNet-0.75, MNASNet-1.3;
		EfficientNet-b2, EfficientNet-b4, EfficientNet-b6; EfficientNet-v2-s, EfficientNet-v2-m, EfficientNet-v2-l [41]
	Transformer	Swin-t, Swin-s, Swin-b [28]

Table 1. The constructed SMR machine library.

According to Eq. (2) and (3), SMR for image classification indicates the proportion of machines that have close class predictions on compressed images or videos with the sources. Images with larger SMRs are better for machine recognition applications because it is more possible to achieve acceptable or correct recognition results on such images. Such advantage becomes more significant when we do not know which machine will be used before the compression, or in a long term that the machine can be upgraded or replaced, both of which are very common in the real world. If the SMR for a compressed image or video frame is precisely determined, we can decide whether it is suitable for machine recognition probabilistically. Then, if the current SMR does not match the expectation, we can change the compression configurations to obtain a larger SMR. Therefore, SMR is a explainable, scalable, and reliable guidance for machine recognition-oriented image and video compression.

### 3. SMR Dataset

In this section, we build the first SMR dataset for SMR studies. There are three steps: image preparation, machine library construction, and SMR annotation.

#### 3.1. Image preparation

First, a large number of high quality and diverse image/video data are needed to build such dataset. Since the images will eventually be used for machine recognition, it is reasonable to utilize existing commonly-used machine vision datasets that have been carefully and professionally constructed. We choose MS COCO [25] 2017 as the source dataset for this work. Although COCO is not specifically designed for image classification, the annotated objects do

have class labels. Therefore, the data volume is further increased because an original COCO image may contain multiple objects. Furthermore, COCO also annotates locations and segmentations for objects, which can be used to study SMR profiles for another two important recognition tasks, *i.e.* object detection and instance segmentation, in the future.

Then, COCO images are compressed as intra video frames by HM-16.24, the reference software of HEVC. To obtain images in different quality levels, 36 quantization parameters are selected for the compression, which are 11, 13, 15, 17, 19, 21 – 51. A larger QP leads to worse image quality. It’s worth mentioning that although HEVC is an video compression standard, it can also be applied to compress images. Furthermore, HEVC is more advanced and capable than most still image compression standards like JPEG because it is powered by several modern compression techniques. Therefore, we can find more generalized and applicable SMR profiles for both images and videos.

#### 3.2. Machine library construction

Obviously, it is impractical to obtain the satisfaction score of every machine in infinite set  $\mathbb{M}$ . Hence, we sample a portion of these machines to form a subset  $\mathcal{M}$  such that

$$SMR_{\mathcal{M}}(I_{q_i}) \simeq SMR_{\mathbb{M}}(I_{q_i}), \mathcal{M} \subset \mathbb{M}. \quad (4)$$

To construct an adequate machine library for the SMR study, we carefully review the growth and current state of the machine community and select several important and representative machines. We build two versions, and the detailed information is presented in Tab. 1, where the leftmost column shows the version of the library. Note that v2 is

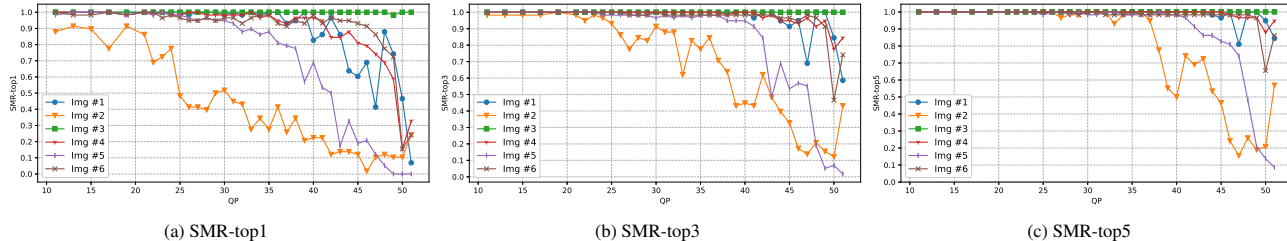


Figure 1. SMR curves of several randomly-selected original images in the SMR dataset.

built upon v1 so it contains all machines from v1. The middle column indicates the coarse-grained category of these machines. The rightmost column shows machines’ names.

The structure, size, and capability of the selected machines differ significantly. For example, their top-1 accuracies on ImageNet [5] range from 60% to 88%, and sizes range from 1.4 to 300 millions of parameters. Hence, they exhibit very distinctive MVS behaviors and can be regarded as independent and equal subjects to obtain the satisfaction scores. The constructed machine library contains 58 and 72 machine subjects in v1 and v2, respectively. The amount of subjects is notably larger when compared to most JND and SUR datasets, such as VideoSet [44] (around 30 human subjects per video) or a more recent and larger-scale dataset [24] (42 subjects per image). Therefore, we believe that it is sufficient to study SMR modeling with this library.

Before annotating SMRs, each selected machine is fine-tuned on the original COCO dataset to recognize COCO objects with initial weights pre-trained on ImageNet from PyTorch [32]. Due to the lack of annotations on the COCO test set, we randomly select 10000 original images from the train set to form the test set. Object images cropped from the entire image according to annotated bounding boxes are used as the selected machines’ inputs, except for those with fewer pixels than  $32 \times 32$  because their semantics may be obscure or broken. The SGD optimizer is used for fine-tuning with cross-entropy loss being the optimization target. The batch size and learning rate are set to 32 and 0.001, respectively, and each machine is trained for 20 epochs (except for ShuffleNets, which require 50 epochs to converge). After fine-tuning, the top-1 accuracies of selected machines range from 78% to 90% on the test set.

### 3.3. SMR annotation

After compression, each original COCO object image has 36 distorted variants. Eq. (2)-(4) are used to annotate the ground truth SMRs for all of them, including the originals. We set  $K = 1, 3, 5$  in Eq. (3), resulting in three types of SMR, namely SMR-top1, SMR-top3, and SMR-top5, respectively. And the two versions of machine library are used separately for annotation. **Eventually, the constructed dataset contains**  $617479 \times (36 + 1) = 22846723$

**images and more than 137 million SMR labels.** There are 20052335, 936396, and 1857992 images for train, validation, and test set, respectively. The data scale is marvelous. We believe that it establishes a solid foundation not only for this work, but also for future SMR studies.

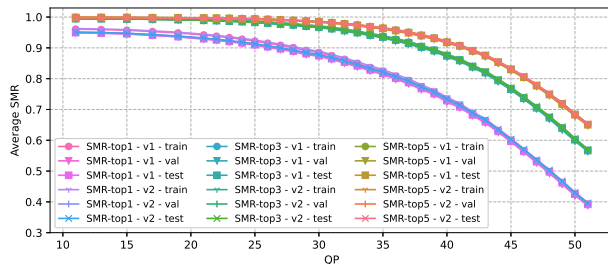


Figure 2. QP-SMR distributions of the SMR dataset.

### 3.4. Dataset analysis

Fig. 1 plots the SMR-top1/3/5 for several randomly-selected images under the selected QPs, which gives a first impression of how SMR curves look like. There are two obvious but important observations. First, different machines do have distinct MVS characteristics because SMR values are not always either 0 or 1. Second, different images also have different SMR profiles.

The average SMRs under different QPs are shown in Fig. 2, where the differences from SMR types (SMR-top1/3/5), machine library versions (v1/v2), and dataset partitions (train/val/test) are all presented. From Figs. 1 and 2, we can draw the following conclusions:

- SMR tends to decrease as QP increases, but the amplitude varies between QPs, and SMRs drop more noticeably at larger QPs. For a certain image, there may be large SMR variations between neighboring QPs.
- SMRs are kept well under shallow compression, but quickly become just acceptable as QP increases, and eventually become unusable under heavy compression.
- SMR distributions for different SMR types are different. At the same QP,  $SMR-top5 \geq SMR-top3 \geq SMR-top1$ . Under small QPs like QP 11,  $SMR-top3/5$

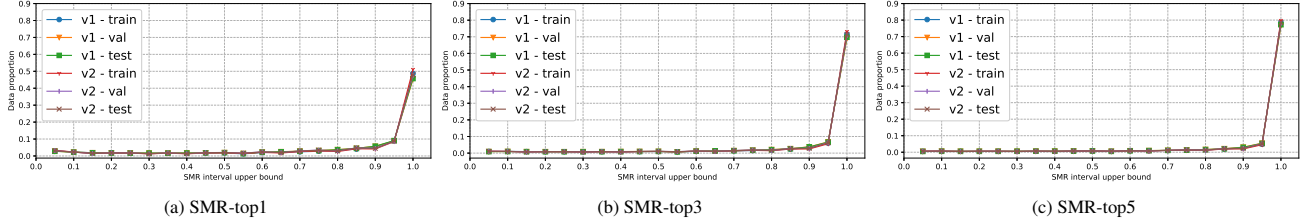


Figure 3. Data proportions of different SMR value intervals in the SMR dataset.

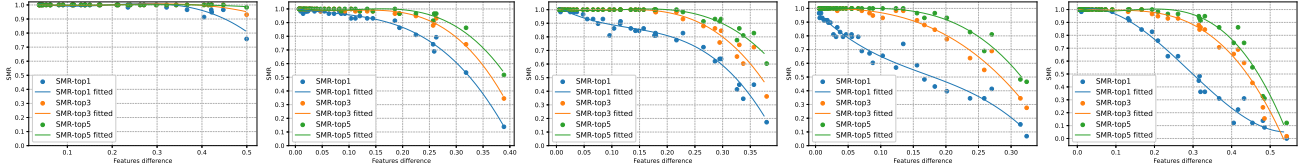


Figure 4. The non-linear negative correlations between mean features difference and SMR for several images in the SMR dataset.

can be close to 1.0 while SMR-top1 cannot. In extreme conditions with a QP near 51, their values are more acceptable than SMR-top1's.

- SMR distributions for different machine library versions are similar. Without counting pristine images, the mean absolute errors (MAE) of SMR-top1/3/5 between v1 and v2 are 0.011, 0.007, and 0.005, respectively, and the standard deviations are 0.024, 0.016, and 0.014 in the constructed dataset. As a result, the established  $\mathcal{M}$  could be a representative subset of  $\mathbb{M}$ .
- SMR distributions for different dataset partitions are similar. An intriguing phenomenon is that the average SMR-top1 is slightly larger in the train set than validation/test set, especially when QP is small. One possible explanation is that the machines are slightly overfitted for the training data, so they perform better on such images. But as QP increases, the impact from image quality degradation becomes more significant than the difference of dataset partitions, thereby the average SMR-top1 becomes closer.

We also count the images in different SMR value intervals, and the results are shown in Fig. 3. The three sub-figures present the data for SMR-top1/3/5, respectively. In each sub-figure, the value on the x axis indicates the upper bound of an SMR interval, with the lower bound determined by the former value. For example, 0.5 indicates (0.45, 0.5]. SMR of 0 is included in the first interval. According to the results, the distribution is imbalanced because most images have large SMRs. More specifically, about 60% of images have a larger SMR-top1 than 0.9. For SMR-top3/5, the proportion is increased to around 75%/85%. **This phenomenon suggests that a large number of pristine images can be heavily compressed without making the majority of machines unsatisfied. Therefore, compression**

**efficiency can be greatly increased.** The compression performance improvement from applying ground truth SMRs will be described in Sec. 5.

## 4. SMR Modeling

For real-world applications, it is necessary to predict the SMR of a specific compressed image or video frame. In this work, a deep learning-based SMR predictor is proposed for such task. Since SMR is a continuous value, the SMR prediction is modeled as a regression task coherently. Moreover, according to Fig. 1, the SMR profile is content-related, so we should model it independently for each image.

Ideally, we would like to have an omnipotent model that can directly output the SMR curve for a pristine image, allowing us to easily determine the optimal operation point for compression. However, it is difficult or even impossible due to the lack of the prior-knowledge about image quality degradation and the machine satisfaction score change. Therefore, we intend to design an SMR prediction model that takes both pristine and compressed image as inputs and estimates the SMR for the compressed image, which is more reasonable and practical.

SMR, as described in Sec. 2, reveals the MVS characteristics of a set of many machines, such as their capabilities and robustness. Since machines understand images and videos by extracting high-level distinguishable features from them, MVS characteristics are embodied during this procedure. Hence, it is reasonable to assume that the SMR of a compressed image is related to the difference between extracted features before and after compression.

Such assumption is verified by plotting the mean features difference and SMR for images in the SMR dataset. Several randomly-selected samples are presented in Fig. 4, where the mean features difference is obtained by averaging the

results from all machines in the v1 machine library, each of which is calculated by the cosine similarity. Note the curves are just fitted cubically as a reference. It can be observed that there is a non-linear negative correlation between these two variables, which can be learned and modeled.

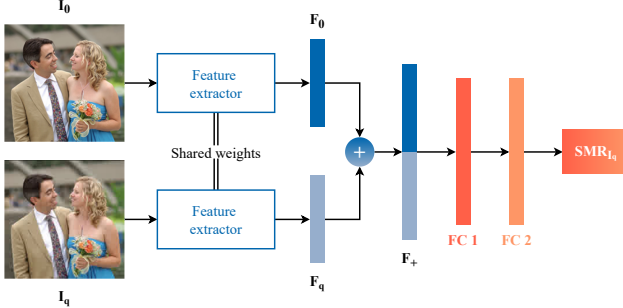


Figure 5. The architecture of the proposed SMR prediction model.

Based on the verification, a simple but effective SMR prediction model powered by deep learning is proposed. Fig. 5 depicts its structure. First, the model uses a neural network to extract features from both pristine and compressed images or video frames, which are denoted as  $F_{I_0}$  and  $F_{I_q}$ , respectively. Second,  $F_{I_0}$  and  $F_{I_q}$  are concatenated to form a high-dimensional feature  $F_+$  that implicitly contains the feature difference information. Finally,  $F_+$  is sent to the fully-connected (FC) layers to output the predicted SMR. Note that we use multiple FC layers along with non-linear activation function layers, which differs from most current neural networks that only have one FC layer, because we want to learn the non-linear correlation of the features difference and SMR as described above.

In the actual implementation, EfficientNet-B4 is chosen as the feature extractor with the initial weights learned on ImageNet. The input and output dimensions of FC layers are  $(1792 \times 2, 3072)$ ,  $(3072, 3072)$ , and  $(3072, 1)$ , respectively. A ReLU module is placed between neighboring FC layers. The entire model is trained on the SMR train set for 10 epochs by the Adam optimizer with batch size set to 252 and learning rate to 0.0001. To avoid any potential effects on an image’s SMR, no data augmentation is used. The regular L1 loss is used as the optimization target.

## 5. Experiments

### 5.1. Evaluation methods and metrics

The prediction error rate is naturally given by the L1 loss. Other than that, we also want to evaluate the compression performance improvement with SMR guidance. Real-world applications would expect compressed images and videos to have larger SMRs than a predetermined threshold. To achieve this goal, they may select a constant QP or bit-rate value for compression based on some prior-knowledges,

such as the QP-SMR distribution shown in Fig. 2. However, compressing with constant QPs cannot reach optimal results because many images or video frames can be compressed with larger QPs without violating the SMR target as explained in Sec. 3.4. Therefore, we use predicted SMRs to improve compression performance in the following steps.

1. We choose a number of possible SMR thresholds to form a set  $\mathbb{T}$ . For each threshold  $T_{SMR}$  in  $\mathbb{T}$ , we select a constant QP with the closest mean SMR to compress  $I_0$  as a baseline, namely  $q_b$ , which is determined from the QP-SMR distribution of SMR dataset.
2. We predict the SMRs of images compressed with  $QP = q_b, q_{b+1}, q_{b+2}, \dots, q_{b+T_q}$  using the proposed model, where  $T_q$  is another customizable threshold indicating the upper bound of applicable QPs. The predicted SMRs are denoted as  $SMR_{pred}(\ast)$ .
3. We search the predicted SMRs reversely to find the first one satisfying  $SMR_{pred}(I_{q_{b+k}}) \geq T_{SMR}$ , and consider  $q_{b+k}$  to be the best QP to compress  $I_0$ .

After that, the average compression rates in bits per pixel (bpp) as well as the mean **actual** SMRs under all SMR thresholds are recorded and compared to the baseline, which forms multiple Rate-SMR curves. The performance is then evaluated by Bjøntegaard Delta rate (BD-rate) [2] and BD-SMR. BD-rate corresponds to the average bit-rate difference **in percent** for the same SMR, the lower the better. BD-SMR corresponds to the average SMR difference for the same bit-rate, the higher the better. Note some source images may have lower SMRs than  $T_{SMR}$  for all QPs in the search interval. In such case,  $q_b$  is used for the compression. The SMR-guided compression scheme should be similar for the constant bit-rate configuration.

### 5.2. Basic results

For experiments, two models are trained on the v1 train set (with annotations from the v1 machine library) to predict SMR-top1/5, respectively. Predicting SMR-top3 should be similar. Fig. 6 shows several predictions (Pred) compared with ground truths (GT). It can be observed that the prediction results are close to the actual SMRs in most cases, even challenging ones, but there are also some failures. On the v1 test set, the MAE between all predicted and actual SMRs can be checked in Tab. 2. Then, we use the method described above to evaluate the compression performance guided by SMR. For SMR-top1,  $\mathbb{T} = [0.5 : 0.05 : 0.95]$ , which means values range from 0.5 to 0.95 with a step size of 0.05. For SMR-top5,  $\mathbb{T} = [0.75 : 0.05 : 0.95]$ . In addition, two kinds of  $T_q$  are introduced as two application strategies. The first (S1) does not limit the upper bound of usable QPs, thereby the largest QP of HEVC (51) can be applied. The second (S2) sets  $T_q = 5$ . The numerical results are shown in Tab. 2 (3rd column), and the Rate-SMR curves are shown in Fig. 7a-7b.

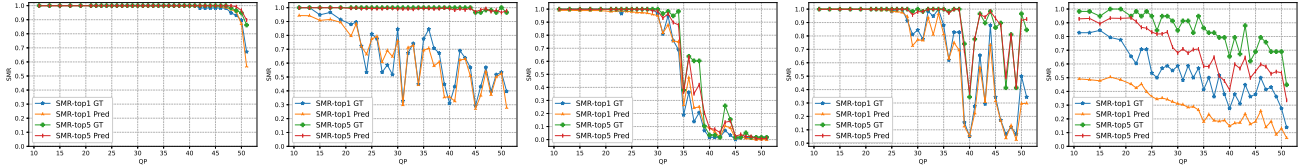


Figure 6. Several randomly-selected predicted SMR curves compared with ground truths in the v1 SMR test set. The predicted SMRs are close to actual ones, even for some challenging images. But there are also failure cases.

	Dataset-Codec	COCO-HEVC		COCO-VVC		COCO-AVS3		VOC-HEVC	
		v1	v2	v1	v2	v1	v2	v1	v2
SMR-top1	Machine library version								
	MAE	0.0463	0.0455	0.0473	0.0531	0.0497	0.0549	0.0371	0.0467
	<b>BD-rate/SMR GT 1</b>	<b>-34.8/0.055</b>	<b>-34.4/0.055</b>	<b>-33.9/0.053</b>	<b>-34.6/0.051</b>	<b>-37.5/0.058</b>	<b>-38.1/0.055</b>	<b>-37.6/0.051</b>	<b>-38.6/0.048</b>
	BD-rate/SMR Pred 1	-25.7/0.038	-27.1/0.040	-23.3/0.034	-24.8/0.035	-28.2/0.040	-29.4/0.041	-27.1/0.034	-28.9/0.035
	BD-rate/SMR GT 2	-26.2/0.034	-26.3/0.033	-25.6/0.032	-25.6/0.031	-26.8/0.033	-26.7/0.032	-28.5/0.029	-28.8/0.027
BD-rate/SMR Pred 2	-21.8/0.027	-22.4/0.028	-21.0/0.026	-21.6/0.026	-22.3/0.027	-22.8/0.027	-24.1/0.024	-24.9/0.023	
SMR-top5	Machine library version								
	MAE	0.0228	0.0222	0.0230	0.0387	0.0262	0.0406	0.0164	0.0350
	<b>BD-rate/SMR GT 1</b>	<b>-43.0/0.085</b>	<b>-43.0/0.086</b>	<b>-42.2/0.080</b>	<b>-42.1/0.074</b>	<b>-43.2/0.081</b>	<b>-42.8/0.076</b>	<b>-47.5/0.082</b>	<b>-47.9/0.075</b>
	BD-rate/SMR Pred 1	-37.1/0.070	-37.7/0.071	-35.9/0.065	-36.6/0.065	-36.9/0.067	-37.4/0.066	-41.9/0.070	-42.7/0.069
	BD-rate/SMR GT 2	-35.9/0.055	-36.0/0.054	-35.1/0.051	-35.0/0.049	-32.7/0.045	-32.3/0.042	-39.0/0.044	-39.2/0.041
BD-rate/SMR Pred 2	-31.3/0.047	-31.8/0.047	-30.1/0.043	-30.7/0.043	-27.9/0.038	-28.2/0.037	-34.4/0.038	-35.1/0.037	

Table 2. The proposed SMR models’ performance on all datasets, machine library versions, and compression frameworks.

Several conclusions can be drawn from the experimental results. (1) Using actual SMRs to guide the QP selection can significantly improve the compression performance. More specifically, the BD-rate savings can be up to 34.8% and 43.0% for SMR-top1 and SMR-top5, respectively. As a reference, the state-of-the-art compression standard VVC outperforms the last-generation standard HEVC by roughly 30% [54]. (2) Using predicted SMRs can also increase the compression efficiency considerably, though not achieving the best performance due to prediction errors. (3) S1 is preferred over S2 for SMR-guided compression. This is because S1 provides a wider range of operation points for compression, where many images can be compressed with QPs inside without lowering SMRs. (4) The performance improvements for SMR-top5 are notably better than SMR-top1 due to much fewer prediction errors.

### 5.3. Generalized to unseen machines

SMR is intended to model MVS behaviors of the general machine community. To verify such generalizability, we evaluate the proposed models on the v2 test set, which contains 14 more machines than v1. Because the models are only trained on the v1 train set, these additional machines are unseen to them. Experimental results are shown in Tab. 2 (4th column) and Fig. 7c-7d. It is interesting to find that MAEs have been even reduced slightly. Along with the fact that the BD-rate and BD-SMR values on v2 are all close to v1, it can be demonstrated that our SMR models have learned generalized knowledge about the universal MVS characteristics. Specifically, the extracted fea-

tures and their differences calculated by the proposed model are not only distinguishable across different image quality levels, but also representative for  $\mathcal{M}$  and probably  $\mathbb{M}$ .

### 5.4. Generalized to unseen compression frameworks

In the real world, applications may use different compression frameworks or codecs. SMR should be adaptable to all of them. To verify such generalizability, we evaluate the proposed models on test sets compressed with various codecs. Despite HEVC that has been tested thoroughly above, we choose VVC and AVS3 for the assessment because they are two state-of-the-art codecs. Their reference softwares, VTM-18.0 and HPM-15.1, are used for the compression. To produce more differences, we increase the internal bit depth to 10 for VVC (as a comparison, both HEVC and AVS3 are using the 8-bit compression configuration). The same QPs for HEVC are still used for VVC because they share the same QP ranges, whereas for AVS3, the selected QPs become 11, 16, 21, 24, 27, 30, 32, 34, 36 – 63. And each  $q_b$  for the corresponding  $T_{SMR}$  in  $\mathbb{T}$  is re-determined for each codec. Furthermore, the evaluation is also carried out on the v2 test set, which challenges the SMR prediction models even more rigorously because they are still trained on HEVC-compressed v1 train set.

Results on VVC- and AVS3-compressed test sets are presented in Tab. 2 (5th-8th columns) and Fig. 7e-7f. Although the MAEs are increased, the compression performance improvements are still remarkable and comparable to the results on HEVC-compressed test sets, which proves the ef-

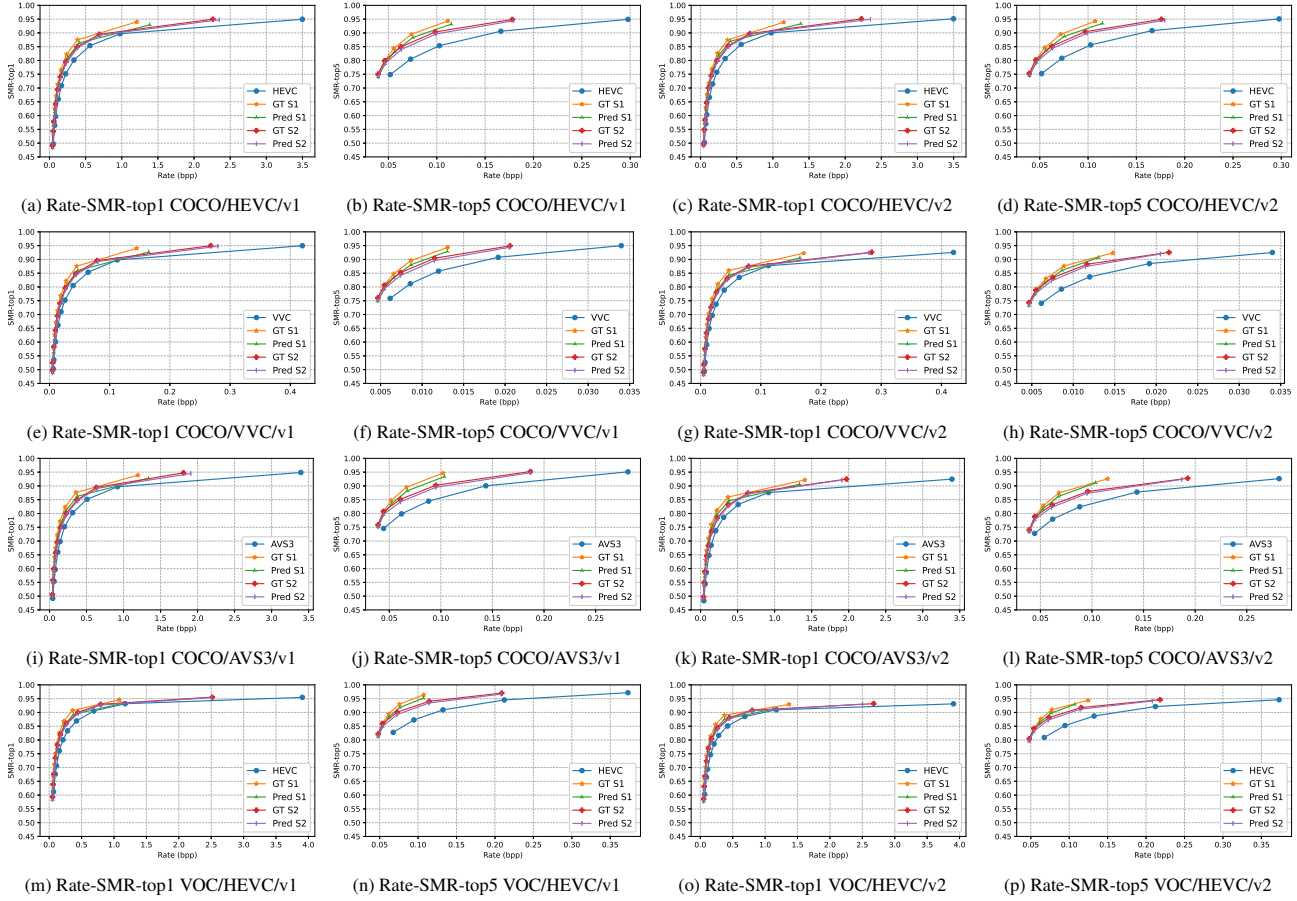


Figure 7. Compression performance improvements using SMR on all datasets, machine library versions, and compression frameworks.

fectiveness of the proposed SMR models on unseen compression frameworks. For each codec, the performance on different versions of machine library is also similar, which again demonstrates the generalizability of SMR models to diverse machines.

As two of the most recent and advanced compression frameworks, VVC and AVS3 significantly outperform HEVC in compression efficiency [54], yet we can still achieve considerable BD-rate savings and BD-SMR increases on these platforms with the proposed SMR model. Therefore, we believe that the SMR model is versatile enough to more codecs, whether more powerful or not, even emerging neural network-based ones, as long as they provide enough operation points. Last but not least, SMR can be a feasible solution for optimizing currently-used compression frameworks to achieve much better efficiency and machine recognition performance while avoiding the cost and risk of replacing them.

## 5.5. Generalized to unseen datasets

Another experiment is conducted for evaluating how SMR models performs on unseen dataset. The test2007 set of PASCAL VOC [7] is chosen as the target, which contains 13315 object images. Note that most object categories of VOC are also included in COCO except "sofa", thereby the semantics of images on these two datasets differ slightly, and the machines in  $\mathcal{M}$  are unaware of them because they are trained on COCO. Tab. 2 (last two columns) and Fig. 7m-7p show the evaluation results, where larger BD-rate savings but slightly smaller BD-SMR gains are observed compared to results on COCO. Since different test data used in Sec. 5.4 is also in another domain for the proposed deep learning-based SMR model, the generalizability of the SMR model to other unseen datasets can be convinced.

## 6. Conclusion

In this paper, we introduce a new concept for machine recognition-oriented image and video compression, namely Satisfied Machine Ratio (SMR). SMR statistically models

the MVS characteristics of the general machine community, making it more reasonable, authoritative, and scalable than other existing MVS-oriented compression methods that only target one or a few machines. We build the first large-scale SMR dataset with over 22 million images for SMR studies, which facilitates future research on this topic. Furthermore, a deep learning-based SMR model is designed to predict the SMR for any given compressed image or video frame. Extensive experiments are conducted to validate the effectiveness of the proposed SMR model, which reveals significant compression and machine recognition performance improvements. In addition, the SMR model generalizes well to different unseen machines, compression frameworks, and datasets. We believe that the proposed SMR model can motivate MVS-oriented visual signal compression from a new perspective. Furthermore, the idea of statistics on MVS behaviors for the general machine community could be extended to other related areas such as quality assessment, adversarial attack, privacy-preserved visual analysis, and more.

## References

- [1] Yuanchao Bai, Xu Yang, Xianming Liu, Junjun Jiang, Yaowei Wang, Xiangyang Ji, and Wen Gao. Towards end-to-end image compression and analysis with transformers. In *Proceedings of the AAAI Conference on Artificial Intelligence*, volume 36, pages 104–112, 2022. 1
- [2] Gisle Bjontegaard. Calculation of average psnr differences between rd-curves. *VCEG-M33*, 2001. 6
- [3] Benjamin Bross, Ye-Kui Wang, Yan Ye, Shan Liu, Jianle Chen, Gary J Sullivan, and Jens-Rainer Ohm. Overview of the versatile video coding (vvc) standard and its applications. *IEEE Transactions on Circuits and Systems for Video Technology*, 31(10):3736–3764, 2021. 1
- [4] Hyomin Choi and Ivan V Bajic. High efficiency compression for object detection. In *2018 IEEE International Conference on Acoustics, Speech and Signal Processing (ICASSP)*, pages 1792–1796. IEEE, 2018. 1
- [5] Jia Deng, Wei Dong, Richard Socher, Li-Jia Li, Kai Li, and Li Fei-Fei. Imagenet: A large-scale hierarchical image database. In *2009 IEEE conference on computer vision and pattern recognition*, pages 248–255. Ieee, 2009. 4
- [6] Alexey Dosovitskiy, Lucas Beyer, Alexander Kolesnikov, Dirk Weissenborn, Xiaohua Zhai, Thomas Unterthiner, Mostafa Dehghani, Matthias Minderer, Georg Heigold, Sylvain Gelly, et al. An image is worth 16x16 words: Transformers for image recognition at scale. *arXiv preprint arXiv:2010.11929*, 2020. 3
- [7] Mark Everingham, Luc Van Gool, Christopher KI Williams, John Winn, and Andrew Zisserman. The pascal visual object classes (voc) challenge. *International journal of computer vision*, 88(2):303–338, 2010. 8
- [8] Chunling Fan, Hanhe Lin, Vlad Hosu, Yun Zhang, Qingshan Jiang, Raouf Hamzaoui, and Dietmar Saupe. Sur-net: Predicting the satisfied user ratio curve for image compression with deep learning. In *2019 eleventh international conference on quality of multimedia experience (QoMEX)*, pages 1–6. IEEE, 2019. 2
- [9] Ruoyu Feng, Xin Jin, Zongyu Guo, Runsen Feng, Yixin Gao, Tianyu He, Zhizheng Zhang, Simeng Sun, and Zhibo Chen. Image coding for machines with omnipotent feature learning. In *European Conference on Computer Vision*, pages 510–528. Springer, 2022. 1
- [10] Kristian Fischer, Fabian Brand, Christian Herglotz, and André Kaup. Video coding for machines with feature-based rate-distortion optimization. In *2020 IEEE 22nd International Workshop on Multimedia Signal Processing (MMSP)*, pages 1–6. IEEE, 2020. 1
- [11] Leonardo Galteri, Marco Bertini, Lorenzo Seidenari, and Alberto Del Bimbo. Video compression for object detection algorithms. In *2018 24th International Conference on Pattern Recognition (ICPR)*, pages 3007–3012. IEEE, 2018. 1
- [12] Wen Gao, Shan Liu, Xiaozhong Xu, Manouchehr Rafie, Yuan Zhang, and Igor Curcio. Recent standard development activities on video coding for machines. *arXiv preprint arXiv:2105.12653*, 2021. 1
- [13] Robert Geirhos, Carlos RM Temme, Jonas Rauber, Heiko H Schütt, Matthias Bethge, and Felix A Wichmann. Generalisation in humans and deep neural networks. *Advances in neural information processing systems*, 31, 2018. 1
- [14] Jingning Han, Bohan Li, Debargha Mukherjee, Ching-Han Chiang, Adrian Grange, Cheng Chen, Hui Su, Sarah Parker, Sai Deng, Urvang Joshi, et al. A technical overview of av1. *Proceedings of the IEEE*, 109(9):1435–1462, 2021. 1
- [15] Kaiming He, Xiangyu Zhang, Shaoqing Ren, and Jian Sun. Delving deep into rectifiers: Surpassing human-level performance on imagenet classification. In *Proceedings of the IEEE international conference on computer vision*, pages 1026–1034, 2015. 1
- [16] Kaiming He, Xiangyu Zhang, Shaoqing Ren, and Jian Sun. Deep residual learning for image recognition. In *Proceedings of the IEEE conference on computer vision and pattern recognition*, pages 770–778, 2016. 3
- [17] Andrew Howard, Mark Sandler, Grace Chu, Liang-Chieh Chen, Bo Chen, Mingxing Tan, Weijun Wang, Yukun Zhu, Ruoming Pang, Vijay Vasudevan, et al. Searching for mobilenetv3. In *Proceedings of the IEEE/CVF international conference on computer vision*, pages 1314–1324, 2019. 3
- [18] Gao Huang, Zhuang Liu, Laurens Van Der Maaten, and Kilian Q Weinberger. Densely connected convolutional networks. In *Proceedings of the IEEE conference on computer vision and pattern recognition*, pages 4700–4708, 2017. 3
- [19] Zhimeng Huang, Chuanmin Jia, Shanshe Wang, and Siwei Ma. Visual analysis motivated rate-distortion model for image coding. In *2021 IEEE International Conference on Multimedia and Expo (ICME)*, pages 1–6. IEEE, 2021. 1
- [20] Nikil Jayant, James Johnston, and Robert Safranek. Signal compression based on models of human perception. *Proceedings of the IEEE*, 81(10):1385–1422, 1993. 2
- [21] Jian Jin, Xingxing Zhang, Xin Fu, Huan Zhang, Weisi Lin, Jian Lou, and Yao Zhao. Just noticeable difference for deep machine vision. *IEEE Transactions on Circuits and Systems for Video Technology*, 2021. 2

- [22] Alex Krizhevsky, Ilya Sutskever, and Geoffrey E Hinton. Imagenet classification with deep convolutional neural networks. *Communications of the ACM*, 60(6):84–90, 2017. 3
- [23] Xin Li, Jun Shi, and Zhibo Chen. Task-driven semantic coding via reinforcement learning. *IEEE Transactions on Image Processing*, 30:6307–6320, 2021. 1
- [24] Hanhe Lin, Guangan Chen, Mohsen Jenadeleh, Vlad Hosu, Ulf-Dietrich Reips, Raouf Hamzaoui, and Dietmar Saupe. Large-scale crowdsourced subjective assessment of picture-wise just noticeable difference. *IEEE transactions on circuits and systems for video technology*, 2022. 4
- [25] Tsung-Yi Lin, Michael Maire, Serge Belongie, James Hays, Pietro Perona, Deva Ramanan, Piotr Dollár, and C Lawrence Zitnick. Microsoft coco: Common objects in context. In *European conference on computer vision*, pages 740–755. Springer, 2014. 3
- [26] Dong Liu, Dandan Wang, and Houqiang Li. Recognizable or not: Towards image semantic quality assessment for compression. *Sensing and Imaging*, 18(1):1–20, 2017. 1
- [27] Huanhua Liu, Yun Zhang, Huan Zhang, Chunling Fan, Sam Kwong, C-C Jay Kuo, and Xiaoping Fan. Deep learning-based picture-wise just noticeable distortion prediction model for image compression. *IEEE Transactions on Image Processing*, 29:641–656, 2019. 2
- [28] Ze Liu, Yutong Lin, Yue Cao, Han Hu, Yixuan Wei, Zheng Zhang, Stephen Lin, and Baining Guo. Swin transformer: Hierarchical vision transformer using shifted windows. In *Proceedings of the IEEE/CVF International Conference on Computer Vision*, pages 10012–10022, 2021. 3
- [29] Zhuang Liu, Hanzi Mao, Chao-Yuan Wu, Christoph Feichtenhofer, Trevor Darrell, and Saining Xie. A convnet for the 2020s. In *Proceedings of the IEEE/CVF Conference on Computer Vision and Pattern Recognition*, pages 11976–11986, 2022. 3
- [30] Sihui Luo, Yezhou Yang, Yanling Yin, Chengchao Shen, Ya Zhao, and Mingli Song. Deepspic: Deep semantic image compression. In *International Conference on Neural Information Processing*, pages 96–106. Springer, 2018. 1
- [31] Ningning Ma, Xiangyu Zhang, Hai-Tao Zheng, and Jian Sun. Shufflenet v2: Practical guidelines for efficient cnn architecture design. In *Proceedings of the European conference on computer vision (ECCV)*, pages 116–131, 2018. 3
- [32] Adam Paszke, Sam Gross, Francisco Massa, Adam Lerer, James Bradbury, Gregory Chanan, Trevor Killeen, Zeming Lin, Natalia Gimelshein, Luca Antiga, et al. Pytorch: An imperative style, high-performance deep learning library. *Advances in neural information processing systems*, 32, 2019. 4
- [33] Ilija Radosavovic, Raj Prateek Kosaraju, Ross Girshick, Kaiming He, and Piotr Dollár. Designing network design spaces. In *Proceedings of the IEEE/CVF conference on computer vision and pattern recognition*, pages 10428–10436, 2020. 3
- [34] Mark Sandler, Andrew Howard, Menglong Zhu, Andrey Zhmoginov, and Liang-Chieh Chen. Mobilenetv2: Inverted residuals and linear bottlenecks. In *Proceedings of the IEEE conference on computer vision and pattern recognition*, pages 4510–4520, 2018. 3
- [35] Karen Simonyan and Andrew Zisserman. Very deep convolutional networks for large-scale image recognition. *arXiv preprint arXiv:1409.1556*, 2014. 3
- [36] Gary J Sullivan, Jens-Rainer Ohm, Woo-Jin Han, and Thomas Wiegand. Overview of the high efficiency video coding (hevc) standard. *IEEE Transactions on circuits and systems for video technology*, 22(12):1649–1668, 2012. 1
- [37] Christian Szegedy, Wei Liu, Yangqing Jia, Pierre Sermanet, Scott Reed, Dragomir Anguelov, Dumitru Erhan, Vincent Vanhoucke, and Andrew Rabinovich. Going deeper with convolutions. In *Proceedings of the IEEE conference on computer vision and pattern recognition*, pages 1–9, 2015. 3
- [38] Christian Szegedy, Vincent Vanhoucke, Sergey Ioffe, Jon Shlens, and Zbigniew Wojna. Rethinking the inception architecture for computer vision. In *Proceedings of the IEEE conference on computer vision and pattern recognition*, pages 2818–2826, 2016. 3
- [39] Mingxing Tan, Bo Chen, Ruoming Pang, Vijay Vasudevan, Mark Sandler, Andrew Howard, and Quoc V Le. Mnasnet: Platform-aware neural architecture search for mobile. In *Proceedings of the IEEE/CVF Conference on Computer Vision and Pattern Recognition*, pages 2820–2828, 2019. 3
- [40] Mingxing Tan and Quoc Le. Efficientnet: Rethinking model scaling for convolutional neural networks. In *International conference on machine learning*, pages 6105–6114. PMLR, 2019. 3
- [41] Mingxing Tan and Quoc Le. Efficientnetv2: Smaller models and faster training. In *International Conference on Machine Learning*, pages 10096–10106. PMLR, 2021. 3
- [42] Robert Torfason, Fabian Mentzer, Eirikur Agustsson, Michael Tschannen, Radu Timofte, and Luc Van Gool. Towards image understanding from deep compression without decoding. *arXiv preprint arXiv:1803.06131*, 2018. 1
- [43] Gregory K Wallace. The jpeg still picture compression standard. *Communications of the ACM*, 34(4):30–44, 1991. 1
- [44] Haiqiang Wang, Ioannis Katsavounidis, Jiantong Zhou, Jeonghoon Park, Shawmin Lei, Xin Zhou, Man-On Pun, Xin Jin, Ronggang Wang, Xu Wang, et al. Videonet: A large-scale compressed video quality dataset based on jnd measurement. *Journal of Visual Communication and Image Representation*, 46:292–302, 2017. 2, 4
- [45] Thomas Wiegand, Gary J Sullivan, Gisle Bjontegaard, and Ajay Luthra. Overview of the h. 264/avc video coding standard. *IEEE Transactions on circuits and systems for video technology*, 13(7):560–576, 2003. 1
- [46] Saining Xie, Ross Girshick, Piotr Dollár, Zhuowen Tu, and Kaiming He. Aggregated residual transformations for deep neural networks. In *Proceedings of the IEEE conference on computer vision and pattern recognition*, pages 1492–1500, 2017. 3
- [47] Wenhan Yang, Haofeng Huang, Yueyu Hu, Ling-Yu Duan, and Jiaying Liu. Video coding for machine: Compact visual representation compression for intelligent collaborative analytics. *arXiv preprint arXiv:2110.09241*, 2021. 1
- [48] Sergey Zagoruyko and Nikos Komodakis. Wide residual networks. *arXiv preprint arXiv:1605.07146*, 2016. 3

- [49] Jiaqi Zhang, Chuanmin Jia, Meng Lei, Shanshe Wang, Siwei Ma, and Wen Gao. Recent development of avs video coding standard: Avs3. In *2019 picture coding symposium (PCS)*, pages 1–5. IEEE, 2019. 1
- [50] Qi Zhang, Shanshe Wang, and Siwei Ma. A novel visual analysis oriented rate control scheme for hevc. In *2020 IEEE International Conference on Visual Communications and Image Processing (VCIP)*, pages 491–494. IEEE, 2020. 1
- [51] Qi Zhang, Shanshe Wang, Xinfeng Zhang, Siwei Ma, and Wen Gao. Just recognizable distortion for machine vision oriented image and video coding. *International Journal of Computer Vision*, 129(10):2889–2906, 2021. 2
- [52] Xiang Zhang, Siwei Ma, Shiqi Wang, Xinfeng Zhang, Huifang Sun, and Wen Gao. A joint compression scheme of video feature descriptors and visual content. *IEEE Transactions on Image Processing*, 26(2):633–647, 2016. 1
- [53] Xinfeng Zhang, Chao Yang, Haiqiang Wang, Wei Xu, and C-C Jay Kuo. Satisfied-user-ratio modeling for compressed video. *IEEE Transactions on Image Processing*, 29:3777–3789, 2020. 2
- [54] Xin Zhao, Shan Liu, Liang Zhao, Xiaozhong Xu, Bin Zhu, and Xiang Li. A comparative study of hevc, vvc, vp9, av1 and avs3 video codecs. In *Applications of Digital Image Processing XLIII*, volume 11510, pages 192–200. SPIE, 2020. 7, 8